Congruent Strategies for Carbohydrate Sequencing. 1. Mining Structural Details by MS n

ARTICLE *in* ANALYTICAL CHEMISTRY · NOVEMBER 2005

Impact Factor: 5.64 · DOI: 10.1021/ac050724z · Source: PubMed

4 AUTHORS, INCLUDING:

Suddham Singh
Pfizer Inc.
39 PUBLICATIONS **863** CITATIONS
SEE PROFILE

Andy Hanneman
Blue Stream Laboratories, Inc.
3 PUBLICATIONS **286** CITATIONS
SEE PROFILE

Vernon Reinhold
University of New Hampshire
106 PUBLICATIONS **4,872** CITATIONS
SEE PROFILE

Published in final edited form as:
Anal Chem. 2005 October 1; 77(19): 6250–6262.

Congruent Strategies for Carbohydrate Sequencing. 1. Mining Structural Details by MS^n

David Ashline, **Suddham Singh**[†], **Andy Hanneman**, and **Vernon Reinhold**[*]
Center for Structural Biology, Department of Chemistry, University of New Hampshire, Durham, New Hampshire 03824

Abstract

This report is the first in a series of three focused on establishing congruent strategies for carbohydrate sequencing. The reports are divided into (i) analytical considerations that account for all aspects of small oligomer structure by MS^n disassembly, (ii) database support using an ion fragment library and associated tools for highthroughput analysis, and (iii) a concluding algorithm for defining oligosaccharide topology from MS^n disassembly pathways. The analytical contribution of this first report explores the limits of structural detail exposed by ion trap mass spectrometry with samples prepared as methyl derivatives and analyzed as metal ion adducts. This data mining effort focuses on correlating the fragments of small oligomers to stereospecific glycan structures, an outcome attributed to a combination of metal ion adduction and analyte conformation. Facile glycosidic cleavage introduces a point of lability (pyranosyl-1-ene) that upon collisional activation initiates subsequent ring fragmentation. Product masses and ion intensities vary with interresidue linkage, branching position, and monomer stereochemistry. Excessive fragmentation is the property of small oligomers where collisional energy within a smaller number of oscillators dissipates through extensive fragmentation. The procedures discussed in this report are unified into a singular strategy using an ion trap mass spectrometer with the sensitivity expected for electron multiplier detection. Although a small set of structures have been discussed, the basic principles considered are fully congruent, with ample opportunities for expansion.

The proliferation of reports attributing biological function to oligosaccaharide epitopes continues unabated. To fully appreciate their specific biological roles, an improved accounting of carbohydrate structural details needs greater scrutiny and more judicious reporting. Unfortunately, a comprehensive strategy for carbohydrate sequencing is lacking. Over the past decades, the absence of an integrated strategy to fully define a carbohydrate sequence has been given little attention due to overwhelming and direct functional lineage of nucleic acid and protein polymers. Even selective strategies to assign components of structure show little focus toward congruency. The reporting of partial sequences, assumed motifs, sequence arrays devoid of linkage and branching definition, and multiple structures enclosed in brackets are currently acceptable conclusions in published reports. The general acceptance of such reports diminishes the driving force for the development of improved and comprehensive methodologies.

A sequence definition should provide all the components of structure necessary for reporting or synthesis. Structural components should include monomer identification, positions of interresidue linkage, and array topology, where a linkage definition includes anomericity, and array topologies describe linear and branching sequence information. When considering molecular glycosylation, sites of conjugation also need to be identified.

[*]Corresponding author. Tel: (603)862-2527. vnr@unh.edu.
[†]Current affiliation: Wyeth-Vaccines, 4300 Oak Park, Sanford, NC 27330.

Numerous reports have discussed alternative strategies for glycan sequencing most frequently using interactive combinations of chromatography and enzymology. We have specifically avoided contrasting these divergent approaches mostly because enzymes frequently fail to define position of release and the secondary need for supporting product characterization. But probably the most important consideration focusing this effort, beyond data quality, is the instrumental simplicity and probability for HTP automation. Mass spectrometry (MS) has continuously proven to be adaptable, and the prospects for improved sensitivity and specificity can be almost assured simply on its past record.

Mass Spectrometry. For defining carbohydrate structure, MS continues to be a key technique that provides both sensitivity and specificity. This expectation, coupled with the ability to generate high-mass gas-phase molecular ions (electrospray ionization, ESI, matrix-assisted laser desorption/ionization, MALDI),[1] strongly suggests MS will continue this dominance. The earlier developments of collisional activation (CA) MS, (introduced as collisioninduced disassociation, CID, by Jennings)[2,3] and tandem MS[4] were interesting adjunct techniques in MS, but the value to biopolymer analysis could not be appreciated until the advances in high-mass ionization. Field desorption, chemical ionization, and fast atom bombardment ionization were interim strategies that provided some direction for solid sample analysis and avoided the pyrolysis of heat vaporization and the high energy of electron bombardment. Both ESI and MALDI produce mainly molecular ions with very little fragmentation; thus, CA has become a major strategy for the characterization of biopolymers. The first indications of the combined power of intact ionization coupled with gas-phase disassembly for carbohydrate materials were reported in 1985[5] using fast atom bombardment (FAB) ionization and two coupled analyzers (BE-EB). FAB ionization and the first analyzer (BE) provided parent ions free from matrix contaminants, and structural detail of these precursors was observed after collision and product ion analysis in a second coupled analyzer (EB). Starting from complex mixtures, this unique instrumental approach, BE-CIDEB, contributed significantly to the GPI anchor structure obtained from human acetylcholinesterase[6] and the analysis of Rhizobial signaling molecules in nitrogen fixation.[7] These exciting structure—functional studies heralded the prospects of gas-phase structural analysis in the absence of chromatography, complete with the sensitivity expected from electron multiplier detection. Developments, however, that have brought the most significant impact to carbohydrate analysis were those leading to the dynamic stabilization of ions in two- and three-dimensional radio frequency quadrupole fields by Wolfgang Paul. These achievements led to the subsequent development of the quadrupole mass spectrometer and the ion trap[8,9] and the 1989 Nobel Prize in physics. Thus, with the ability to ionize samples at high mass and observe fragments by CA in Paul ion traps, all the components were in place for a full and detailed investigation of carbohydrate structure. The first commercially available IT instruments were sold in 1984, but it was another decade, when combined with ESI, that carbohydrate analysis moved beyond the early success with triple quadrupole instruments. First early reports demonstrated the advantages of ITMS, but little attention was focused on defining the limits of understanding carbohydrate structure.

Methylation. Derivatization has been a mainstay of oligosaccharide structural investigations for over a century. Effective analysis requires quantitative blocking of all hydroxyl groups, a goal difficult to achieve, and that probably relates more to the solubility of the reactants than the chemistry of the functional groups. This aspect is rarely observed directly due to the extensive organic extraction and washes with water that successfully remove many polar undermethylated products. The first *O*-methyl ethers of carbohydrate samples were prepared by Purdie and Irvine[10] using methanolic solutions treated repeatedly with methyliodide and silver oxide. Denham and Woodhouse[11] and Haworth[12] reported comparable results a few years later using dimethyl sulfate and sodium hydroxide. The popular Purdie technique was significantly improved by Kuhn and co-workers,[13] who carried out the reaction in the polar solvent *N*,*N*-dimethylformamide. All methods, however, gave partially methylated products

and approached completion only with repeated steps. Hakomori[14] demonstrated full methylation in one step using sodium methylsulfinyl carbanion and methyl iodide dissolved in dimethyl sulfoxide (DMSO). This method remained the procedure of choice for another decade. The most recent improvement, and clearly the simplest approach, has been that of Ciucanu and Kerek.[15] To a sample dissolved in DMSO, they added a slurry of sodium hydroxide followed by methyl iodide. The overall simplicity and the relatively low spectral background have now made this method the most popular. Over the years, methylation has resolved a number of major structural problems and along with acetylation has dominated the Haworth—Birmingham carbohydrate school for years. Haworth's application of methylation provided a whole range of crystalline well-characterized methyl ethers and their oxidized products clarified Fischer ring structures, resolving the 20-year Haworth—Hudson controversy. This stemmed from the assumption that the isomeric methyl glycosides discovered by Emil Fischer in 1893 were to have five-membered, oxygencontaining rings, a point disproved by Haworth and his associates by methylation, which established a six-membered, oxygen-containing ring. Hudson claimed the methylation strategy altered the ring structure and the solution invalid and sought unsuccessfully to determine the true ring structure by correlation of structure and optical rotation. More contemporary applications were methylation analysis to characterize methylated alditol acetates by GC/MS.[16] Thus, mass spectrometry was combined with methylation quite early, first to stabilize structures from the more energetic ionization procedures, second for the advantages provided by sample cleanup using lipophilic extraction, and finally for the enhanced ion signals. Unraveling the details of structure by CID and the advantages provided by methylation has been an evolving process aided significantly by improved instrumentation. Such combinations provided the structural details of a GnT-I metabolite,[17] profiling EPO Lys-C digests and their N- and O-linked glycans structures,[18] defining Rhizobial exopolysaccharide binding epitope,[19] lipid A metabolites,[20] GSL structures,[21–23] and unraveling a unique bacterial endoglycosidase O-linked glycan structure.[24] Many of these reports have been summarized.[25,26]

The simple principle of derivatizing all available hydroxyls within an oligosaccharide and characterizing the products following fragmentation has not changed, and we extend that principle in this report using ITMS instrumentation for disassembly and characterization.

Metal Ion Adduction. It is generally assumed that no single analytical technique would be capable of a complete oligosaccharide characterization. Even within a single instrumental approach, there are multiple options that can define specific features. Collision analysis of lithium adducts[27] or negative ion extraction[28] provides impressive linkage details, but comprehensive sequence topology, monomer, and terminal information remains incomplete. Compared to protonation, Cerny et al.[29] demonstrated that collisional activation of sodiated oligosaccharides provides a larger number of structurally informative fragments, and Cancilla et al.,[30] has reported the binding energy of alkali metals decreases in the order Li > Na > K > Rb > Cs. Botek et al.[31] recently described ab initio calculations for formation enthalpies with glucose and a stability order $Li^+ > Na^+ > K^+$. The calculations and modeling confirmed a twisted boat conformation with all cations coordinated to the same four oxygen atoms and an ion yield approximating a 4-fold enhancement over sodium when using lithium adduction. Metal—oxygen binding affinity would be enhanced with sample methylation due to hyperconjugation, and methylation has been shown to influence sample volatility and hydrophobicity with a consequent 20-fold higher ion yield for the sodium adduct of tetramethylglucose.[31] We have compared these cations and noted lithium′s greater affinity throughout MS^n, as evidenced by enhanced ion abundance; however, ratios for similar fragments were not constant and strongly suggest stereospecific binding may also contribute to ion abundance and not physical parameters exclusively.

Molecular Disassembly. Developments leading to high mass ionization in the absence of fragmentation focused the greater need for improved techniques of oligomer depolymerization. Enzymatic proteolysis has largely filled this void for proteins, and peptide mass fingerprints are a sustaining technology for characterization. Comparable endoglycosidases are rare, but more importantly, oligomers exist with multiple isobars (GlcNAc and GalNAc; Man, Glc, and Gal), and the transparency of linkage and branching makes a simple MS^2 fingerprint approach elusive. In addition, presumptive amino acid sequences can be obtained from genomic information, whereas no such analogous sequence or linkage message is available for oligosaccharides. Over the decades the literature is replete with chemical attempts (acid, base, reductive, oxidative) for partial oligosaccharide depolymerization with the hope of sequence overlap to define a single topological array. None has proven sustainable, and invariably polymer degradation and stereochemical damage precludes any universally useful applications. But the greatest complications arise from the need to characterize stereochemical features to the smallest units that will identify isomeric monomers and the stereochemistry of its linkage. Collisional activation has added significantly to disassembly, but the constrained level of energy delivered in a single analysis (MS/MS) fails to capture the diversity of structural details in large oligomers, and higher energies fragment to such a degree that molecular continuity is lost. The ion trap, with its sequential approach to disassembly (MS^n), effectively proportions higher energy to smaller oligomers, allowing a cross section of bonds to be probed in detail with molecular continuity tracked by the precursor-product relationships in every step. This fundamental feature of the ion trap is based on the quasi-equilibrium theory, which states that available pathways for energy dissipation by fragmentation is inversely proportional to the number of oscillators. Consistent with that principle, we explored structure—fragment relationships of small methylated oligomers and pursued the limits of informative fragmentation in linear and Paul ion traps. Methylation fixes structural features and exposes points of rupture throughout disassembly, principles that add significantly to ion product understanding.

This report is the first in a series of three integrated accounts that endeavor to identify congruent sequencing strategies to capture all components of carbohydrate structure by MS^n. They include multistage disassembly (this report), computational tools to compile, search, and compare fragment data files,[32] and finally a concluding report describing an algorithm that assimilates the spectral data into an array topology that together aspires to provide all components of structure.[33] Glycans were profiled by ESI mass spectrometry in both linear and Paul traps (MS^n).

EXPERIMENTAL METHODS

Methods and Sample Preparation. Maltose, maltotriose, panose, globotriose, and Gal-α (1-4)-Gal were purchased from Sigma (St. Louis, MO). Cellotriose, linear B2 trisaccharide, (Gal-α(1-3)-Gal-β(1-4)-GlcNAc), lacto-*N*-tetraose, lacto-*N*-neotetraose, and lacto-*N*-fucopentaose I were purchased from Calbiochem (EMD Biosciences, Inc., La Jolla, CA). Nigerotriose and laminaritriose were purchased from V-Labs, Inc. (Covington, LA). Selected oligosaccharides were reduced with $NaBH_4$ (10 mg/mL, dissolved in 0.01 M NaOH) and left overnight at room temperature. The reduction solution was chilled, terminated by the addition of glacial acetic acid, and diluted with 3 mL of ethanol before drying under a nitrogen stream. Borate esters were removed by repeated addition and drying of a 1% acetic acid methanol solution. Three milliliters of toluene was added and evaporated three times. The dried samples were dissolved in water, desalted by passage through a column of Dowex 50W cation-exchange resin (Sigma-Aldrich, St. Louis, MO), and redried. Methylation was carried out according to the method of Ciucanu and Kerek.[15] Briefly, the samples were dissolved in DMSO (HPLC grade, Sigma-Aldrich), followed by addition of powdered sodium hydroxide (99.999%, Sigma-Aldrich). After vortexing to produce a suspension, iodomethane (99.5%, Sigma-Aldrich) was

added. The reaction tube was then vortexed for 1 h to allow the reaction to proceed. Afterward, water was added to stop the reaction. Permethylated oligosaccharides were extracted three times with dichloromethane (HPLC grade, EMD Biosciences, Inc.). The extracts were combined and washed three times with MilliQ water (Millipore Corp., Billerica, MA). The dichloromethane was evaporated under nitrogen stream. Native (unmethylated) and methylated samples were dissolved in methanol/water (1:1, containing 1 mM sodium acetate) for mass spectrometry. Mass spectrometry experiments were carried out on a linear ion trap mass spectrometer (LTQ, ThermoFinnigan, San Jose, CA) using a nanoelectrospray source, 0.40-0.60 μL/min flow rate at 200-230 °C capillary temperature in positive ion mode with 30-50% collision energy. Selected studies were also carried out by MALDI-QIT-TOF (Axima-QIT, Kratos Shimadzu, Manchester, UK), using dihydroxybenzoic acid as a matrix. Collision energies were set to leave a small but detectible abundance of the precursor ion. Activation *Q* and activation time were left at their default values, 0.25 and 30 ms, respectively, for all MS^n experiments. In our experience, changing collision energy will affect the relative abundance of precursor ion, but generally does not change the relative product ion abundances. Changing the activation *Q* or activation time can affect relative product ion abundances and so were kept constant. All ions were sodium adducts, except where noted.

RESULTS AND DISCUSSION

Methylation, Pyranosylenes, and Retro-Diels-Alder Degradation. Primary fragments of a methylated oligomer yield two basic fragment types as a consequence of cleavage at the glycosidic bond producing the reducing and nonreducing termini (B- and Y-ions).[34] Other single bond fragments (usually at much lower abundance) occur adjacent to the glycosidic bond, which are identified as the C- and Z-type ions. A second set of fragments, also of lower abundance, are the important two bond cleavages (across the ring) that define linkage position (Scheme 1). The respective structures at the point of cleavage are the pyranosyl-1-ene (B-ions) and an open hydroxyl (Y-ions).[17,24] Product ions of equivalent *m/z*, (isobars) are frequently observed in the collision spectra due to ion constitution (monomer order), linkage variations (interresidue linkage position), or solely on the basis of stereochemistry (monomer identity and anomeric configuration).

Reducing terminal ions (Y-ions) are often more abundant, but it is the B-ions that are more informative when probed by MS^n analysis. This important feature relates directly to their collisional instability and the generation of stereospecific ring fragments. Pyranose unsaturation (as in B-ions) coupled with metal ion chelation appears to lower the energy barriers to ring rupture via a classical retro-Diels-Alder (RDA) decomposition reaction.[35–37] In support of a RDA pathway and to corroborate the proposed gas-phase structure, organic synthesis of a pyranosyl-1-ene (pyranosylene)-containing disaccharide was undertaken. Comparative product analysis (MS^2) provided an identical spectrum.[38] Thus, it appears that the introduction of a double bond provides the π electrons to support chemical rupture via RDA and collisional activation supplies the energy to complete the process. The stereospecificity observed may be a consequence of metal ion chelation, and of the RDA reaction itself, which is known to retain such structural features.[37] Under such conditions, the product masses will vary depending on linkage position to the pyranosylene ring and the ion intensities will vary depending on the stereochemistry of chelation. As described below, methylation also contributes to RDA degradation, and this feature may be entwined with the specificity and avidity of metal ion binding.[31] We have assumed these factors to be fundamental for the detection of configurationally diagnostic fragment ions and have provided supporting data below.

CID of the methylated disaccharides Gal-α(1-4)-Gal and Glc-α(1-4)-Glc (*m/z* 477) provided nearly identical spectra with major B- and C-type fragments at *m/z* 241 and *m/z* 259, along with an ion at *m/z* 445, produced by loss of methanol (Figure 1A and B, respectively). Certainly,

as methyl glycosides, these small oligomers appear relatively stable to ring fracture, and as a consequence, no linkage or monomer characterization is evident. Consistent with the instability of pyranosylenes, we prepared the same disaccharide in Figure 1B as its unsaturated counterpart, Glc-α(1-4)-Glc(1-ene), and compared the native and methylated samples by MS^3 analysis (Figure 2A and B, respectively). Note that the spectrum of the native sample Glc-α(1-4)-Glc(1-ene) can yield two fragments of equal mass, but even as a B-type fragment, the only bond rupture was at the glycosidic linkage with little hint of ring instability. The peak at *m/z* 329 in the native spectrum results from water loss. In clear distinction were the MS^3 spectra of the methylated analogues. These precursors show abundant RDA reaction products and strong supporting evidence for a sequencing strategy that includes methylation and fragmentation of B-ion precursors. The abundant peak at *m/z* 329.1 and the trace ion at *m/z* 315.1 are cross-ring cleavage fragments while the ions at *m/z* 259.0, 209.0, 227.0, and 241.0 are products of interlinkage rupture from both sides of the glycosidic oxygen. The peaks at *m/z* 413 and 415 probably result from loss of methanol and formaldehyde, respectively. While permethylated structures typically do not lose water, they do tend to lose methanol, formaldehyde, or both, which we generally find to be uninformative. The methylated sample yields several fragments of different mass, enabling an easy differentiation of each monomer for further MS^n characterization without complicating isobars. The importance of methylation in its contribution to RDA degradation was apparent in additional samples with different monomers and linkages. When a fragment of lacto-*N*-fucopentaose, Fuc-α(1-2)-Gal(1-ene), was analyzed by MS^3 as the native and methylated derivative, the latter analogue again showed abundant cross-ring and glycosidic cleavages while the former exhibited mainly the glycosidic cleavage (Figure 3).

Characterization of Linkages. Linkage details within larger methylated glycans and oligosaccharides have been previously reported,[25,39] but contributing features and the limits of structural detail were not rigorously pursued. To probe and contrast these features in methylated B-ions, we selected two milk tetrasaccharides, lacto-*N*-tetraose, Gal-β(1-3)-GlcNAc-β(1-3)-Gal-β(1-4)-Glc, and lacto-*N*-neotetraose, Gal-β(1-4)-GlcNAc-β(1-3)-Gal-β(1-4)-Glc. The tetrasaccharides possess differently linked terminal disaccharides, Gal-β(1-3)-GlcNAc and Gal-β(1-4)-GlcNAc, with the same anomeric configuration and monomer composition. The profiled tetrasaccharides, *m/z* 926, were isolated and analyzed by MS^2, which generated the B-type fragments (*m/z* 486) in both samples, Gal-β(1-3)-GlcNAc(1-ene) and Gal-β(1-4)-GlcNAc(1-ene) (Figure 4A and B, respectively). Analysis of these pyranosylene disaccharides in MS^3 showed the cross-ring cleavage fragments at *m/z* 412 as the major ion, for the Gal-β(1-3)-GlcNAc(1-ene) structure along with C- and Z-type fragments at *m/z* 259 and 250. The major ion at *m/z* 444 attributed to loss of an acetyl group. In contrast, MS^3 analysis of the alternatively linked Gal-β(1-4)-GlcNAc(1-ene) product showed a different cross-ring cleavage ion at *m/z* 329, along with a major ion at *m/z* 444 (loss of an acetyl group), and C- and Y-types ions at *m/z* 259 and 268. Interestingly, the ion at *m/z* 456 in Gal-β(1-4)-GlcNAc(1-ene) was due to the loss of formaldehyde, and it was not observed in the CID spectra of Gal-β(1-3)-GlcNAc(1-ene).

In a second sample with linkage-specific differences, the pyranosylene (B-type) ions Glc-α(1-4)-Glc(1-ene) and Glc-α(1-6)-Glc(1-ene) were isolated from the trisaccharides maltotriose (Glc-α(1-4)-Glc-α(1-4)-Glc) and panose (Glc-α(1-6)-Glc-α(1-4)-Glc). These trisaccharides were first reduced to avoid any possibility of generating an isobaric Z-ion disaccharide. The MS^3 spectrum of the substructure, Glc-α(1-4)-Glc(1-ene) (Figure 5A) shows cross-ring cleavage ions at *m/z* 315 and 329. However, MS^3 of Glc-α(1-6)-Glc(1-ene) (Figure 5B) shows only the cross-ring cleavage ion *m/z* 329. Both fragments show the C-type fragment *m/z* 259 and ions at *m/z* 415 (loss of formaldehyde) and 413 (loss of methanol). Intensity differences were also notable among the common ions in both examples. These fragment differences are clearly represented by different linkage position and may be, in part, explained by the RDA

reaction initiated from the pyranosylene terminus. Scheme 1A shows a generic 1,4-linked B_2-type Hex-Hex ion that undergoes the RDA reaction to yield a *m/z* 329 ion. The *m/z* 139 ion is generally a low-abundance ion or is absent from these spectra, presumably due to the larger fragments greater affinity for the metal ion charge carrier. Scheme 1B shows generic cross-ring cleavage ions that may be seen as fragments generated from B-ions corresponding to the various linkages. Collisional activation appears to induce bond migration providing a small amount of other pyranosylenes. This prior to RDA may account for the multiple products (Scheme 1B). Not all fragments are present. For example, ^{0,4}A fragments from 1,6-linked oligosaccharides are more likely to occur if the pyranosylene ring is part of a branch, as in N-linked glycans. In the example shown in Figure 5B, Glc-α(1-6)-Glc(1-ene), this ion is absent. ^{0,4}A fragments from 1,4-linkages generally do not occur if the pyranosylene is a hexose, but may be a low-abundance peak if the pyranosylene is a HexNAc. The actual masses will depend on the identity of the monomers; i.e., fucose, hexoses, and *N*-acetylhexosamines, in various combinations, yield fragments of various mass even though the type of cleavage may be similar.

Characterization of Monomers within Disaccharides. To understand how monomer stereochemistry influences dimer fragmentation, the B-type fragments Gal-α(1-4)-Gal(1-ene) and Glc-α(1-4)-Glc(1-ene) were generated by MS^2 analysis of the reduced, permethylated trisaccharides globotriositol (Gal-α(1-4)-Gal-β(1-4)-Glc-ol) and maltotriositol (Glc-α(1-4)-Glc-α(1-4)-Glc-ol) (Figure 6A and B, respectively). In general, the fragment masses are the same in each spectrum with the galactosylene analogue showing a major cross-ring fragment at *m/z* 329 and a smaller ion at *m/z* 315 (Figure 6A). Interresidue fragments are observed at *m/z* 227 (Y-ion), 241 (B-ion), and 259 (C-ion). The glucosylene analogue (Figure 6B) generated comparable ion masses, but with a significantly different pattern of intensities. For Gal-α(1-4)-Gal(1-ene), the *m/z* 329 fragment was the most intense ion with a set of ions approximating one-quarter of its intensity: *m/z* 413, 259, 415, 227, 415, 257, 315, and 241. For Glc-α(1-4)-Glc(1-ene), *m/z* 259 was the most intense ion, followed by *m/z* 329 and 413. The remaining fragments, *m/z* 257, 415, 209, 227, 315, and 241, were around 10% of the base ion. This seems to suggest that the galactose analogue was more susceptible to RDA degradation (cross-ring cleavage) than a glycosidic cleavage (e.g., *m/z* 329 is considerably more intense than the *m/z* 259 peak). In the case of Glc-α(1-4)-Glc(1-ene), the opposite seems to be the case. These spectral differences are reproducible, suggesting that these intensity patterns relate to the monomer stereochemistry. Until we have a better understanding of metal ion binding and its influence on electron delocalization or stabilization it would be premature to propose a mechanism for these intensity differences. Preliminary modeling of such structures, coupled with synthesis of intermediates, has provided an improved understanding, but conclusions must be corroborated with more extensive studies currently ongoing.

These small reproducible spectral differences in an α(1-4) linked galactose and glucose homodisaccharides were also observed with an α(1-3) interresidue linkage (Figure 7). The starting trisaccharide for the glucosylene dimer was nigerotriose (Glc-α(1-3)-Glc-α(1-3)-Glc) and, for the galactosylene analogue, linear B2 trisaccharide (Gal-α(1-3)-Gal-β(1-4)-GlcNAc). Again, both spectra have many fragments of the same mass with some similarities in the pattern of intensities, particularly for *m/z* 413, 371, 259, and 415. A set of more intense ions at *m/z* 383, 343, 315, 241, and 211 in the galactosylene spectrum provides ample difference for characterization. As in the spectra of Figure 6, these intensity differences are reproducible. As previously indicated, we are currently unable to explain in a detailed mechanistic way the reasons for these spectral differences. However, we can empirically see that these structural differences give rise to mass spectral differences, and such differences can be used in library matching of unknowns with standard oligosaccharides. Figures 6 and 7 show the putative effect of the reducing end monomer since all cross-ring fragments can be readily explained as involving the monomer with the double bond.

By identifying fragments from this adisaccharide study, all linkage positions could be assigned and the reducing end monomer characterized. An additional observation important for the characterization of 2-linked B-type ions is that they do not generate C-type ion products. This probably relates to the fact that an E2 elimination (of C-ions) requires the reactant to acquire a point of unsaturation that cannot be accommodated at C_2 with sp^2 hybridization. Although the details of stereospecific fragmentation will continue to unravel with further study, two limitations remain; first is a failure to define isomers that require an unmodified configuration at C_2. This is because a B-type fragment loses stereospecificity at carbon 2 (sp^2 at C_2); thus, mannose, glucose, altrose, and allose lead to an identical structure, and in the same manner, galactose becomes stereoisomeric with gulose, idose, and talose. Second, the monomer at the nonreducing terminus of disaccharides eliminates intact and remains uncharacterized. However, these latter monomers can be isolated as C-type ions and analyzed by MS^4 (discussed below). The isomers missed in B-ion formation are rarely a problem in practice either by their absence in an isomeric sequence or by their scarcity in nature.

Characterization of Isolated Monomers, B-Ions. Although reducing end monomer information is lost in the generation of pyranosylenes, for numerous samples, B-ions provide an effective and direct strategy for the differentiation of nonreducing terminal galactose from glucose or mannose. As an example, to fully characterize the disaccharide samples prepared for Figure 6, the nonreducing hexose was isolated as the B-ion for MS^4 analysis. Such an approach was also applied to the samples of maltotriose (Glc-α(1-4)-Glc-α(1-4)-Glc) and globotriose (Gal-α(1-4)-Gal-β-(1-4)-Glc). In this experiment, lithium was used as the adduct, and the disassembly sequence *m/z* 681 → 429 → 225 provided the B-ion representing the nonreducing terminal hexose (Figure 8A and B, respectively). We have noted that lithium adducts both of the RDA cross-ring cleavage products, and their relative ratio is an exacting measure for the characterization of these isomers. Data have been compiled for the terminal hexoses of many oligosaccharides and are presented for sodium adducts (Table 1) and lithium adducts (Table 2). In each table, we indicate the identity of the terminal monomer, the parent compound, and the fragmentation pathway used to obtain the B_1-ion. The final column in each table gives a relative intensity of the putative dienophile fragment (*m/z* 125 for the sodium adduct, *m/z* 109 for the lithium adduct) to the putative diene fragment (*m/z* 139 for the sodium adduct, *m/z* 123 for the lithium adduct) for the various monomers. The relative intensity of the putative dienophile fragment is significantly greater for galactose residues than for glucose or mannose residues. This difference is also more striking when lithium is used as the metal ion adduct. Typical relative intensities for glucose and mannose residues were less than 2.5% for lithium adducts, while for galactose relative intensities are generally ~40%. The relative ion intensities of the diene and dienophile marker ions may be related to putative differences in their ability to coordinate the metal ion charge carrier.

It is well known that the Diels-Alder reaction is stereospecifically syn with respect to the dienophile, thus leading to the different cis/trans isomers of the *m/z* 125 (sodiated) or 109 (lithiated) fragments of glucose/mannose and galactose. By the principle of microscopic reversibility, the reverse reaction should follow the same mechanism as the forward reaction. Specifically, galactose would yield *cis*-1,2-dimethoxyethene ((Z)-1,2-dimethoxyethene) while glucose and mannose would yield *trans*-1,2-dimethoxyethene ((E)-1,2-dimethoxyethene), as shown in Figure 8. Presumably, talose, idose, and gulose could also yield a *cis*-1,2-dimethoxyethene fragment, but these sugars are rarely seen in the important naturally occurring oligosaccharides. The tables also provide an example of reproducibility and how these lithium ratios appear to be uniform. We presume that the smaller lithium ion is less able to coordinate the oxygen atoms of the *trans*-1,2-dimethoxyethene as compared to sodium. The apparent relatively greater preference of lithium to coordinate the *cis*-1,2-dimethoxyethene (compared to sodium) may be due to the possible preference of sodium for more than two coordination sites, such that it is more likely to coordinate the diene fragment. Regardless, the empirical

data suggest that we can reliably distinguish galactose from glucose or mannose in this way; distinguishing glucose from mannose requires investigation of C-type ions.

Characterization of Isolated Monomers, C-Ions. In selected cases where it may be necessary to differentiate terminal glucose from mannose, sodiated C-type fragments may offer a better alternative. An analysis of C-ions of glucose generated from reduced, permethylated maltotriose and mannose from unreduced, permethylated Man-β(1-4)-GlcNAc, as well as glucose from reduced, permethylated nigerotriose and mannose from reduced, permethylated mannobiose (Man-α(1-3)-Man), are presented in Figure 9A-D, respectively. The patterns of fragment masses are similar, while the intensities differ for each monomer, regardless of the monomer′s precursor. This further suggests metal ion chelation may assist or be involved in stereoselective fragmentation. Currently, the pathways of degradation are not as clear for C-type fragments as for B-type fragments, so accounting for structural relationships must await further study. However, the similarity in the pattern of intensities for the major ions for the same monomer from different precursors indicates that spectral library matching is feasible.[32]

Characterization of Anomers. Anomeric configuration is a more challenging structural feature to characterize. The reduced, permethylated trisaccharides maltotriose and cellotriose were prepared to compare the isobaric B-ion disaccharide fragments Glc-α(1-4)-Glc(1-ene) and Glc-β(1-4)-Glc(1-ene) at *m/z* 445 (Figure 10). In both spectra, the fragment masses were generally similar and reproducible, but clearly exhibited small intensity differences in the ions at *m/z* 413, 415 and 227, suggesting structural relationships. Interestingly, the -30 and -32 fragments showed considerable differences in this case, but these losses are not yet well defined. However, not all comparable pyranosylenes showed only minor differences. The fragments from nigerotriose and laminaritriose B-ions were more pronounced, and it is tempting to relate these patterns to structures, but the details must await further study (Figure 11). There is no obvious reason to not expect a specific pathway of degradation (as observed for B-type ions and the RDA reaction) for selective isomersf that could serve as markers of anomericity.

CONCLUSIONS

This report explores the limits of structural detail (linkage, monomer identification, and anomeric configuration) exposed by ion trap mass spectrometry and links these strategies in a single methodological approach. Gas-phase disassembly to small oligomers indicates all details of structure are observed for the requirements of synthesis and detailed reporting. Stereoselective details are dependent on sample methylation and metal ion adduction. Although multiple corridors of disassembly are available, it is only a selective few that exhibit structurally relevant information and study of these ions has exposed understandable reaction mechanisms. Much of that detail was observed within pyranosylene (B-type) ion structures, which readily fragment in a stereospecific manner by a retro-Diels-Alder reaction. Efforts in our laboratory have also used these reliable cross-ring cleavages and MS^n fragment pathways to develop a computer algorithm to determine glycan structures in a de novo fashion.[33] In other cases, fragmentation mechanisms are not yet well defined, such as in C-type ions, yet demonstrable differences in spectra can be seen. These putative stereospecific mass fragments and abundance ratios has made substructure library matching possible.[32] Such considerations of marker ions and pathway continuity may allow progression toward total structures in the form of a bottom-up sequencing strategy. The use of ion pathways and ion trees may obviate the need for chromatography as the product precursor relationships are known through MS^n disassembly. Top-down analysis of the initial branches obtained in MS^2 and MS^3 will be combined with the spectral matching approach to yield a congruent strategy for total structure determination at unmatched sensitivity.

ACKNOWLEDGMENT

The work was supported by NIH grants GM 45054 (V.R.), NCRR-BRIN grant RP016459 (V.R.), and NCRR-COBRE grant P20 RR16437 (William Green, DMS) shared equipment grants from Dartmouth Medical School and the University of New Hampshire.

References

(1). Cook KD. Am. Soc. Mass Spectrom 2002;13:1359.

(2). Jennings K. Int. J. Mass Spectrom. Ion Phys 1968;1:227.

(3). Haddon WF, McLafferty FW. J. Am. Chem. Soc 1968;90:4745.

(4). Futrell J, Miller C. Rev. Sci. Instrum 1966;37:1521.

(5). Carr SA, Reinhold VN, Green BN, Hass JR. Biomed. Mass Spectrom 1985;12:288–295. [PubMed: 3160406]

(6). Roberts WL, Santikarn S, Reinhold VN, Rosenberry TL. J. Biol. Chem 1988;263:18776–18784. [PubMed: 2848807]

(7). Spaink HP, Sheeley DM, van_Brussel AA, Glushka J, York WS, Tak T, Geiger O, Kennedy EP, Reinhold VN, Lugtenberg BJ. Nature 1991;354:125–130. [PubMed: 1944592]

(8). Paul W, Steinwedel HZ. Naturforsch 1953;8A:448.

(9). Paul W. Angew Chem., Int. Ed. Engl 1990;29:739.

(10). Purdie T, Irvine JC. J. Chem. Soc. (London) 1903;83:1021–1037.

(11). Denham WS, Woodhouse H. J. Chem. Soc. (London) 1913;103:1735.

(12). Haworth WN. J. Chem. Soc (London) 1915:8–16.

(13). Kuhn R, Trischmann H, Low I. Angew Chem., Int. Ed. Engl 1955;67:32.

(14). Hakomori S-I. J. Biochem. (Tokyo) 1964;55:205. [PubMed: 14135466]

(15). Ciucanu I, Kerek F. Carbohydr. Res 1984;131:209.

(16). Bjorndal H, Hellerquist HG, Lindberg B, Svensson S. Angew Chem., Int. Ed. Engl 1970;9:610.

(17). Velardo MA, Bretthauer RK, Boutaud A, Reinhold B, Reinhold VN, Castellino FJ. J. Biol. Chem 1993;268:17902–17907. [PubMed: 8349674]

(18). Linsley KB, Chan SY, Chan S, Reinhold BB, Lisi PJ, Reinhold VN. Anal. Biochem 1994;33:207–217. [PubMed: 8080078]

(19). Reinhold BB, Chan SY, Reuber TL, Marra A, Walker GC, Reinhold VN. J. Bacteriol 1994;176:1997–2002. [PubMed: 8144468]

(20). Chan S, Reinhold VN. Anal. Biochem 1994;33:63. [PubMed: 8053569]

(21). Reinhold BB, Chan S-Y, Chan S, Reinhold VN. Org. Mass Spectrom 1994;29:736–746.

(22). Stroud MR, Handa K, Ito K, Salyan ME, Fang H, Levery SB, Hakamori S, Reinhold BB, Reinhold VN. Biochem. Biophys. Res. Commun 1995;209:777–787. [PubMed: 7537499]

(23). Stroud MR, Handa K, Salyan ME, Ito K, Levery SB, Hakomori S, Reinhold BB, Reinhold VN. Biochemistry 1996;35:770–778. [PubMed: 8547257]

(24). Reinhold BB, Hauer CR, Plummer TH, Reinhold VN. J. Biol. Chem 1995;270:13197–13203. [PubMed: 7768917]

(25). Reinhold VN, Reinhold BB, Costello CE. Anal. Chem 1995;67:1772–1784. [PubMed: 9306731]

(26). Reinhold VN, Reinhold BB, Chan S. Methods Enzymol 1996;271:377–402. [PubMed: 8782562]

(27). Zhou Z, Ogden S, Leary JA. J. Org. Chem 1990;55:5444.

(28). Chai W, Lawson AM, Piskarev VJ. Am. Soc. Mass Spectrom 2002;13:670–679.

(29). Cerny RL, Tomer KB, Gross ML. Org. Mass Spectrom 1986;21:655–660.

(30). Cancilla MT, Penn SG, Carroll JA, Lebrilla CB. J. Am. Chem. Soc 1996;118:6736–6745.

(31). Botek E, Debrun JL, Hakim B, Morin-Allory L. Rapid Commun. Mass Spectrom 2001;15:273–276. [PubMed: 11223958]

(32). Zhang H, Singh S, Reinhold VN. Anal. Chem 2005;77:6163–6270. [PubMed: 16194074]

(33). Ashline D, Singh S, Hanneman A, Reinhold VN. Anal. Chem 2005;77:6250–6262. [PubMed: 16194086]

(34). Domon B, Costello CE. Glycoconjugate J 1988;5:397–409.

(35). Biemann K. Angew Chem., Int. Ed. Engl 1962;1:98–111.

(36). Kwart H, King K. Chem. Rev 1968;68:415–433.

(37). Mandelbaum, A. In Applications of Mass Spectrometry to Organic Stereo-chemistry. Splitter, J.; Turecek, F., editors. VCH Publishers Inc.; 1993. p. 299-324.

(38). Zhou, H.; Zercher, C.; Reinhold, VN. Personal communication. 2005.

(39). Sheeley DM, Reinhold VN. Anal. Chem 1998;70:3053–3059. [PubMed: 9684552]

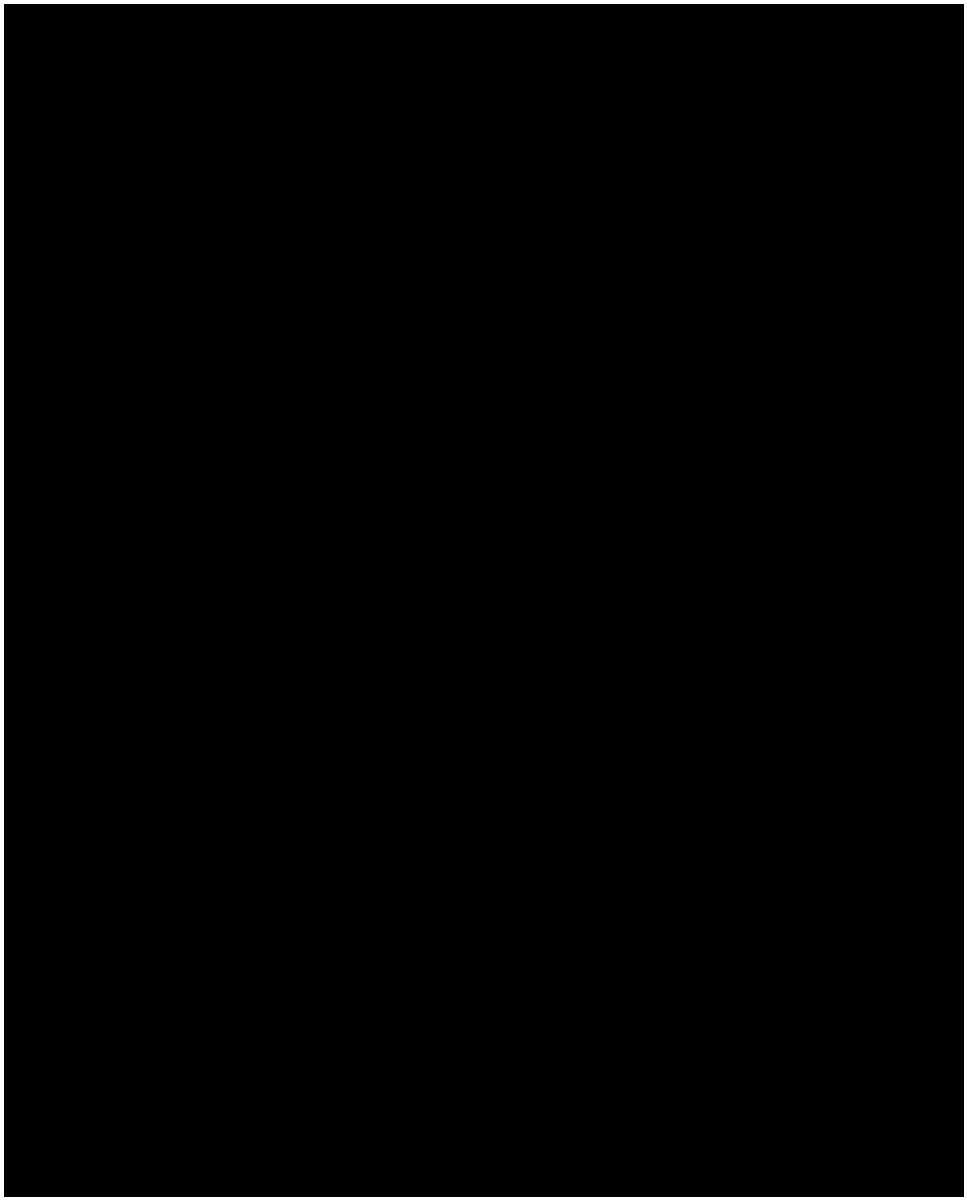

Scheme 1.

Example of a retro-Diels—Alder reaction in a 1,4-linked B_2-type Hex-Hex disaccharide, showing formation of an *m/z* 329 ion from an *m/z* 445 ion (A). The *m/z* 139 ion is generally of low abundance or absent, presumably due to the larger fragments stronger affinity for the metal ion charge carrier. (B) shows the generic cross-ring cleavages that may be formed from B-type ions of various linkages. R indicates the location of mono- or oligosaccharide substituents.

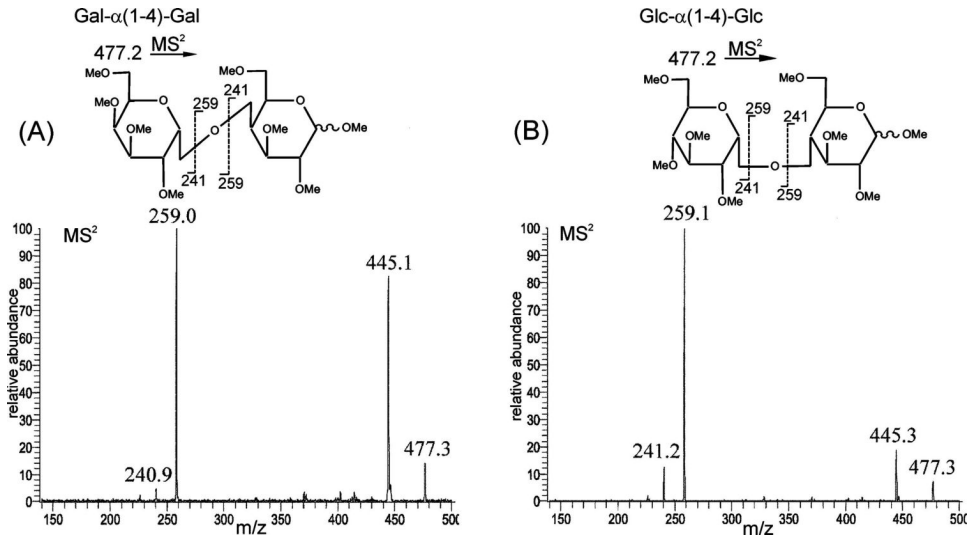

Figure 1.

ESI-MS^2 spectra of methylated disaccharide isobars composed of different monosaccharides. (A) Gal-α(1-4) Gal and (B) Glc-α(1-4) Glc. The absence of unsaturation, as in B-ions, results in little fragment specificity.

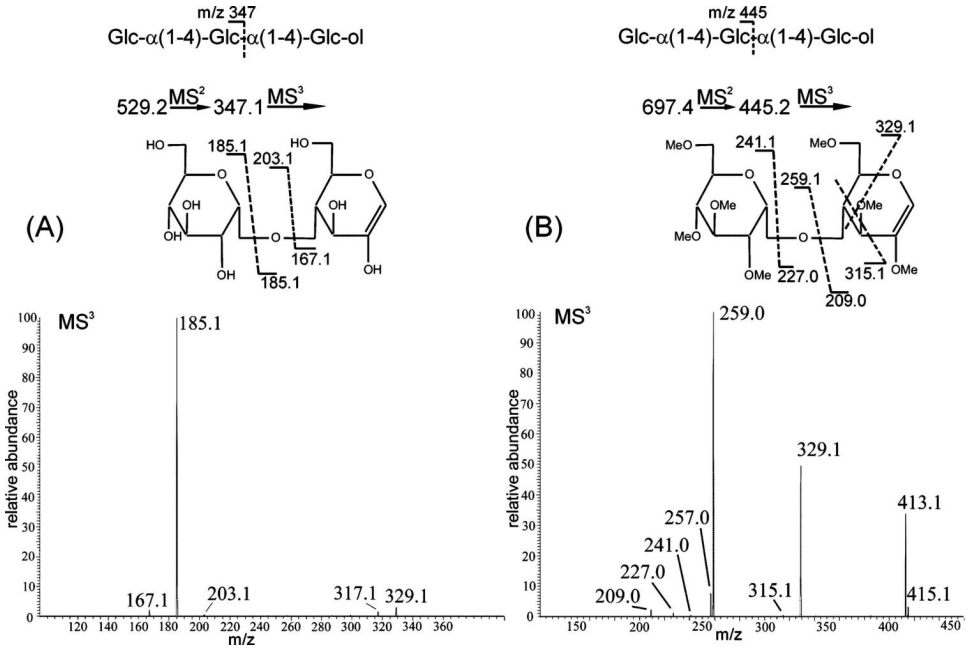

Figure 2.

ESI-MS^3 spectral comparison of native (A) and methylated (B) B_2-type fragment of maltotriositol. Comparative results demonstrate importance of methylation and unsaturation (e.g., Figure 1) providing precursor ion favorable to extensive fragmentation.

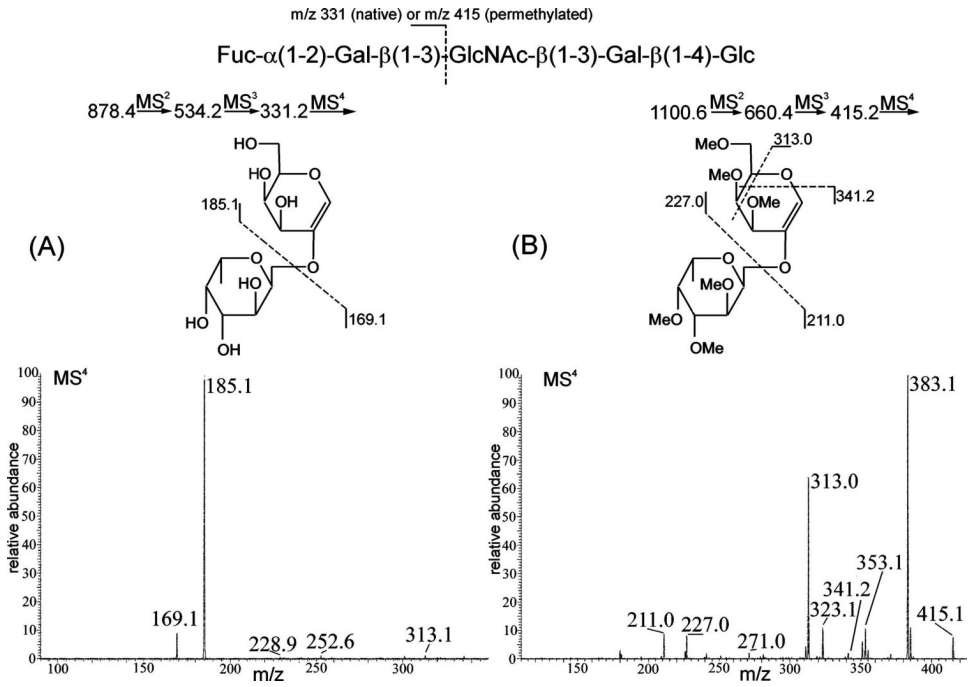

Figure 3.

ESI-MS^3 spectral comparison of native (A) and methylated (B) B_2-type fragment of tetrasaccharide milk glycan lacto-*N*-fucopentaose I. Note the prominent cross-ring cleavage fragment in the permethylated sample.

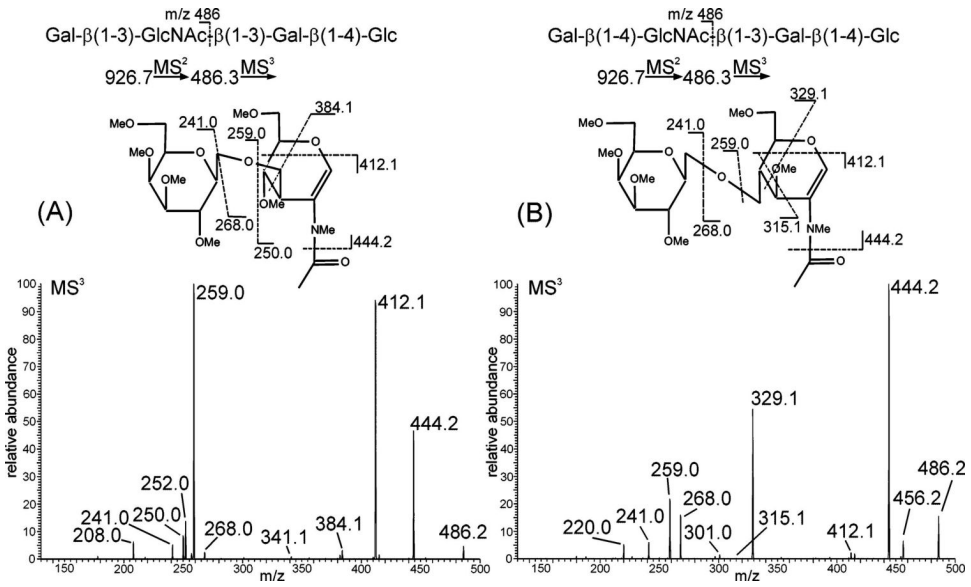

Figure 4.

ESI-MS^3 spectral comparison of B_2-type fragments of the tetrasaccharides (A) lacto-$_N$-tetraose and (B) lacto-$_N$-neotetraose. Note the different fragments present in each spectra, arising from the different linkages.

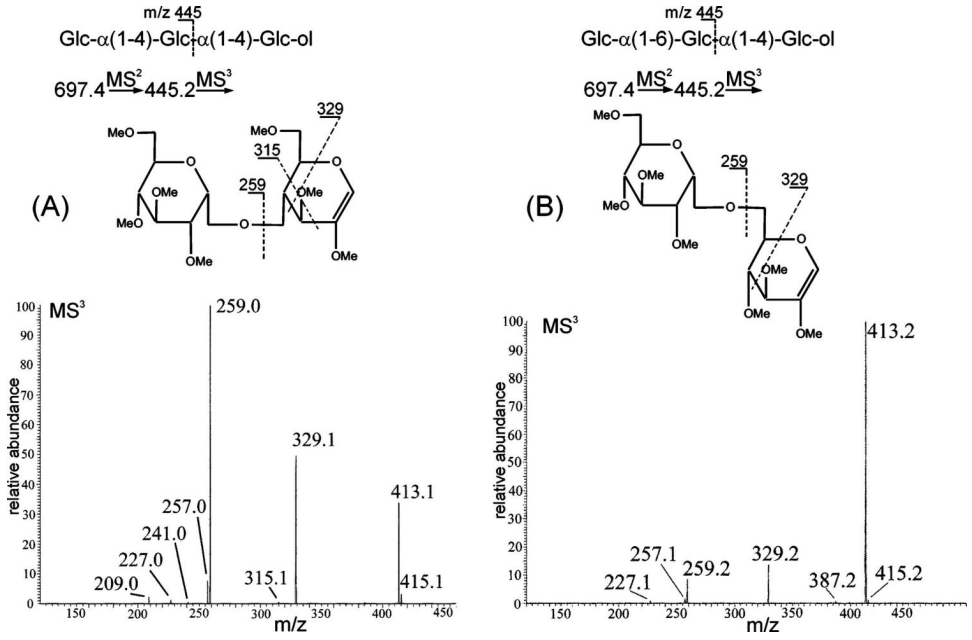

Figure 5.

ESI-MS^3 spectral comparison of B_2-type fragments of reduced, methylated trisaccharides (A) maltotriose and (B) panose. The presence of the cross-ring cleavage fragment at *m/z* 315 in the Glc-α(1-4)-Glc(1-ene) fragment, along with the *m/z* 329 fragment, is indicative of a 1-4 linkage, while the presence of only a *m/z* 329 cross-ring cleavage fragment (and absence of *m/z* 315) is indicative of a 1-6 linkage in panose.

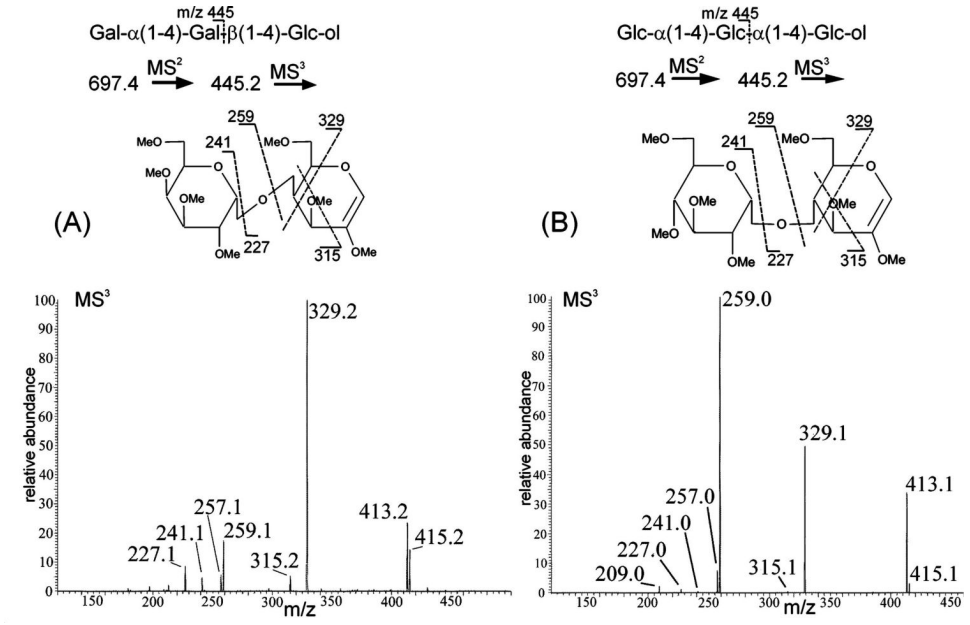

Figure 6.

ESI-MS^3 spectral comparison of the effect of monomer identity on B_2-type fragment spectra from reduced, methylated trisaccharides. (A) globotriose vs (B) maltotriose. Note the different pattern of intensities on spectra collected on the same instrument.

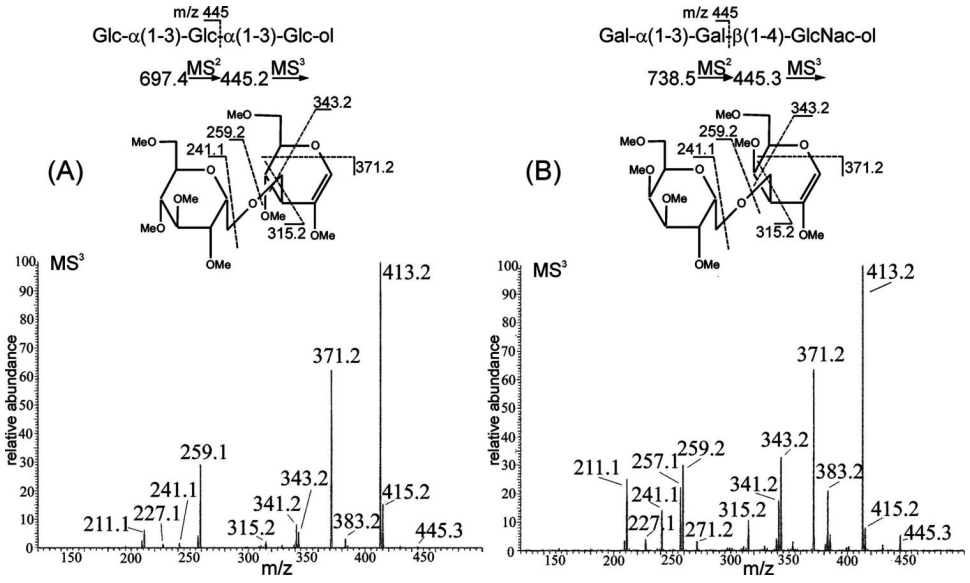

Figure 7.

ESI-MS^3 spectral comparison of effect of monomer identity on B_2-type fragment spectra from reduced, methylated trisaccharides. (A) nigerotriose vs (B) linear B2 trisaccharide. Note the different pattern of intensities seen on spectra obtained with the same instrument.

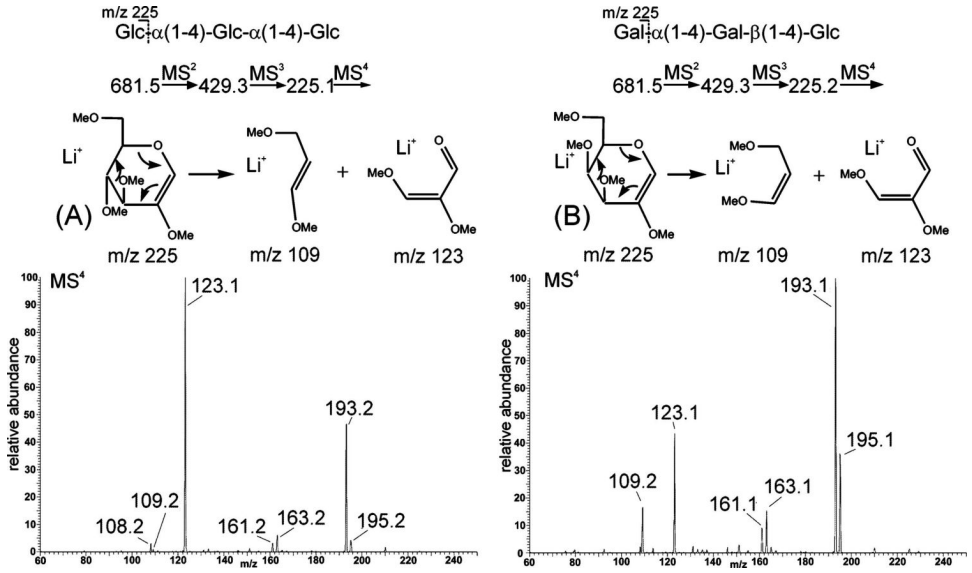

Figure 8.

ESI-MS^4 spectral comparison of different B_1-type fragment spectra from reduced, methylated trisaccharides. (A) maltotriose (glucose) vs (B) globotriose (galactose). Note the more prominent *m/z* 109 fragment in the galactose spectra.

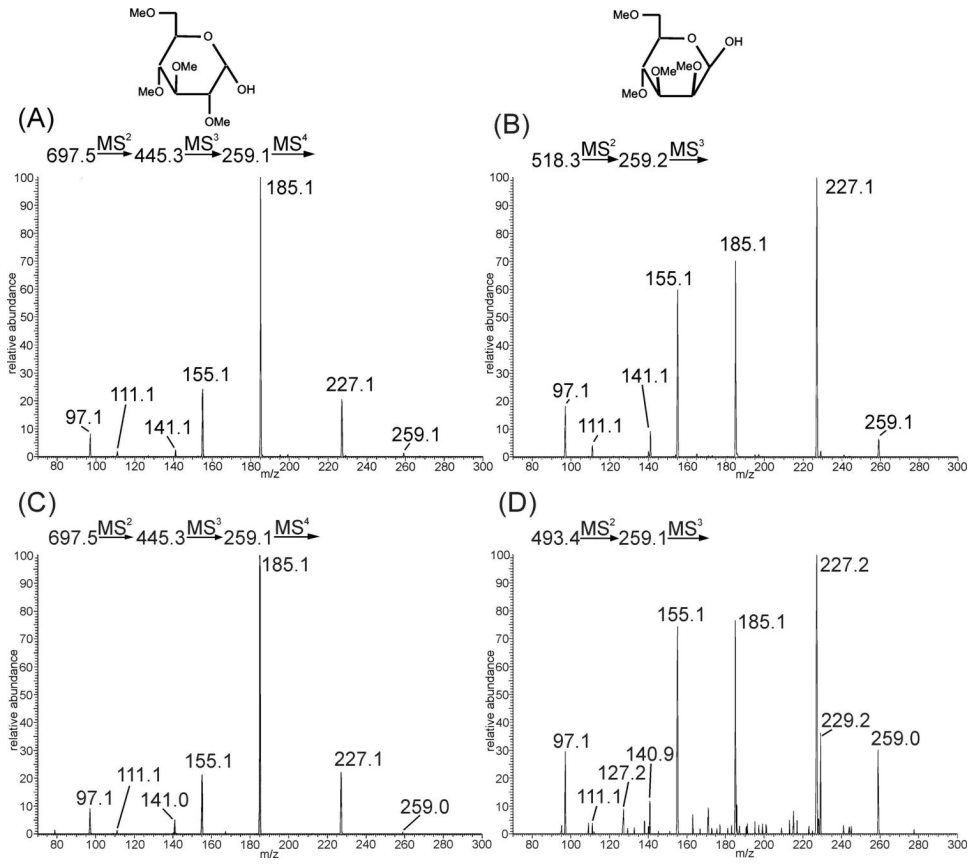

Figure 9.

ESI-MS^n spectral comparison of C_1-type fragments of reduced, methylated maltotriose (A), unreduced, methylated Man-β(1-4)-GlcNAc (B), nigerotriose (C), and mannobiose (D). Note the different pattern of intensities between glucose (A, C) and mannose monomers (B, D) and the similarity of (A) and (C) vs (B) and (D).

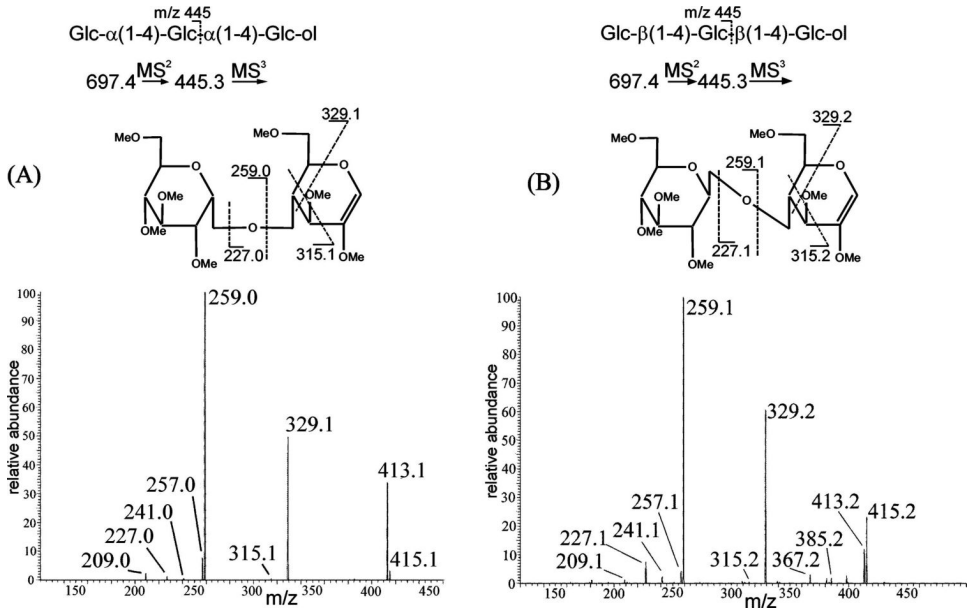

Figure 10.

ESI-MS^3 spectral comparison of anomeric configuration on B_2-type fragment spectra from reduced, methylated trisaccharides. (A) maltotriose vs (B) cellotriose. Note the slightly different pattern of intensities.

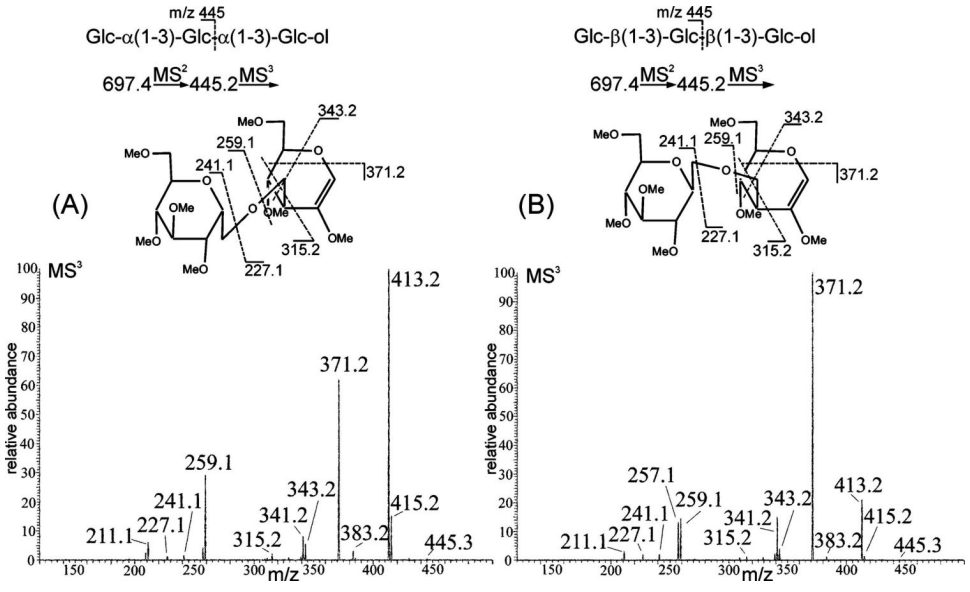

Figure 11.

ESI-MS^3 spectral comparison of anomeric configuration on B_2-type fragment spectra from reduced, permethylated trisaccharides. (A) nigerotriose vs (B) laminaritriose. Note the different pattern of intensities.

Table 1.

Relative Intensities of *m/z* 125/*m/z* 139 for Terminal B1 Monomers as Their Sodium Adducts[a]

monomer	parent	path	rel intens, % (125/139) × 100
glucose	maltotriose	697.5 → 445.3 → 241.1	0.00
mannose	Man-β(1-4)-GN, unreduced	518.4 → 241.1	0.22
glucose	synthetic, permethylated glucosylene	241	0.27
mannose	Man-α(1-3)-Man, reduced	493.3 → 241.1	0.59
glucose	cellotriose, reduced	697.5 → 445.3 → 241.1	0.92
glucose	synthetic maltose-1-OAc	505.4 → 445.1 → 241.1	1.09
glucose	nigerotriose, Glc-α(1-3)-Glc-α(1-3)-Glc	697.4 → 445.3 → 241.1	1.59
glucose	maltose, reduced	493.3 → 241.1	2.22
glucose	cellobiose, reduced	493.3 → 241.1	2.59
mannose	Man-α(1-6)-Man, reduced	493.3 → 241.1	2.96
galactose	GN413 (Gal-β(1-3)-GalNAc-β(1-4)-Gal-β(1-4)-Glc)	926.7 → 486.3 → 241.1	9.01
galactose	Gal-β(1-4)(Fuc-α(1-3))-GlcNAc-β(1-3)-Gal-β(1-4)-Glc	1100.7 → 454.2 → 241.1	9.09
galactose	melibiose, reduced	493.3 → 241.1	10.08
galactose	Gal-β(1-3)-GlcNAc-β(1-3)-Gal-β(1-4)-Glc	926.5 → 486.3 → 241.1	10.40
galactose	Gal-α(1-6)-GlcNAc, unreduced	518.3 → 241.1	11.31
galactose	lactose, unreduced	477.3 → 241.1	12.79
galactose	Gal-β(1-3)-Ara, reduced	449.4 → 241.1	13.09
galactose	linear B2 trisaccharide	738.5 → 445.3 → 241.1	16.39
galactose	globotriose, Gal-α(1-4)-Gal-β(1-4)-Glc	697.4 → 445.2 → 241.2	20.27

[a]Relative intensity was calculated by dividing the intensity of the *m/z* 125 peak by the intensity of the *m/z* 139 peak and multiplying by 100.

Table 2.

Relative Intensities of *m/z* 109/*m/z* 123 for Terminal B1 Monomers as Their Lithium Adducts[a]

monomer	parent	path	rel intens, % (109/123) × 100
mannose	Man-β(1-4)-Glc-β1-Ceramide	1022.8 → 447.3 → 225.0	0.3
mannose	Man-β(1-4)-GlcNAc	502.4 → 225.2	0.3
glucose	synthetic maltose-1-OAc	489.3 → 429.2 → 225.2	0.5
mannose	Man-β(1-4)-Glc-β1-Ceramide	994.8 → 447.3 → 225.1	0.7
glucose	synthetic maltose-1-Obn	537.4 → 429.2 → 225.1	0.7
glucose	maltotriose	681.5 → 429.3 → 225.2	0.8
mannose	man-α(1-3)-man	477.4 → 225.1	0.9
glucose	maltose	477.4 → 225.2	2.5
galactose	Gal-β(1-4)(Fuc-α(1-3))-GlcNAc-β(1-3)-Gal-β(1-4)-Glc	1084.6 → 438.2 → 225.2	37.2
galactose	globotriose	681.5 → 429.3 → 225.1	38.3
galactose	novel C. elegans glycan	1243.6 → 1056.5 → 417.1 → 225.2	38.9
galactose	Gal-α(1-3)-Gal-β(1-4)-Glc-β1-Cer	1339.0 → 651.4 → 429.3 → 225.2	39.1
galactose	Gal-β(1-4)-Glc-β1-Cer	994.9 → 447.3 → 225.1	40.2
galactose	linear B2 trisaccharide	722.5 → 429.3 → 225.1	38.2

[a]Relative intensity was calculated by dividing the intensity of the *m/z* 109 peak by the intensity of the *m/z* 123 peak and multiplying by 100.